Scientific Research Publishing

Open Journal of Physical Chemistry, 2024, 14, 61-81
https://www.scirp.org/journal/ojpc
ISSN Online: 2162-1977
ISSN Print: 2162-1969

Polyoxometalate Supported on Bentonite as Efficient Adsorbent for the Removal of Methylene Blue Dye and Bacteria from Wastewater

Abrar Iskandrani[1,2], Afra M. Baghdadi[3], Fatma Bannani[1]

[1]Department of Chemistry, College of Science, University of Jeddah, Jeddah, Saudi Arabia
[2]Department of Chemistry, College of Science, King Abdulaziz University (KAU), Jeddah, Saudi Arabia
[3]Department of Biological Sciences, College of Science, University of Jeddah, Jeddah, Saudi Arabia
Email: fatmabannanidriss@gmail.com

How to cite this paper: Iskandrani, A., Baghdadi, A.M. and Bannani, F. (2024) Polyoxometalate Supported on Bentonite as Efficient Adsorbent for the Removal of Methylene Blue Dye and Bacteria from Wastewater. *Open Journal of Physical Chemistry*, **14**, 61-81.
https://doi.org/10.4236/ojpc.2024.144005

Received: October 22, 2024
Accepted: November 26, 2024
Published: November 29, 2024

Abstract

Aiming at developing benign multiple decontamination water adsorbent, using low-cost natural raw local materials, we prepared a modified Bentonite supporting polyoxometalate ionic liquid composite hybrid, where each component targets a specific type of water contaminant. The composite material based on water-insoluble polyoxometalate-ionic liquid (POM-IL) consisting of antimicrobial tetraoctylammonium cations, and saturated Keggin-archetype polyoxometalate $[PV_3W_9O_{40}]^{6-}$ anions, immobilized on Bentonite having an interesting dye removal capacity. The $Q^8[PV_3W_9O_{40}]$@Bentonite (Q^8 = TetraOctylAmmonium), composite was tested for cationic dye removal from waste water. Batch experiments for the adsorption of Methylene Blue MB were conducted to investigate the effect factors containing the initial concentration, contact time, adsorbent amount, pH and Temperatures. According to the results of the kinetic study, the pseudo-second-order model fitted better the adsorption experimental data compared to the first order model. The experimental isotherm data were found to fit the Langumir model well compared to the Freundlich model. The thermodynamic parameters illustrated that the adsorption process was endothermic and spontaneous. The results of the present study showed that modified Bentonite represents an excellent multicomponent low-cost adsorbent for the removal of cationic dye and Bacteria from waste water.

Keywords

Adsorption, Bentonite, Polyoxometalates, Ionic Liquid, Antibacterial,

Wastewater Treatment

1. Introduction

Wastewater contamination has emerged as a major environmental challenge in many countries, largely due to industrial development [1] [2]. Dye contaminants, toxic inorganic substances such heavy metals and hazardous bacteria are behind this pollution. Organic, non-biodegradable dyes consisting of conjugated chromophores and fused aromatic rings are considered as the worst type of water contaminants [3] [4]. Dyes are viewed as a significant risk to human health and environment as a result of their toxicity, carcinogenicity and potential mutagenicity, and the discharge of the dyes without treatment into the environment can also inhibit the penetration of sunlight into the water, which leads to the die-off of plants and animals [5] [6]. Methylene Blue, as a typical cationic dye, was predominantly chosen as a model organic dye to examine the adsorption process due to its wide range application in textile industries [4]. Before discharging toxic dyes into the environment, it is highly recommended to treat wastewater containing dye pollutants using proper treatment method (**Table 1**) [7]. Among these methods, adsorption is considered as an economical and efficient process to treat this dye. The efficiency of the adsorption process depends on choosing the appropriate adsorbent. The selected adsorbent should be easily abundant and low cost [8].

Table 1. The types of wastewater treatment.

Physical treatment	Adsorption electrochemical technique ion-exchange membrane filtration
Physicochemical treatment	reverse osmosis chemical oxidation ozonation coagulation flocculation
Biological treatment	bacterial action activated sludge

Natural Bentonite have been considered as adsorbent which meets the above-mentioned characteristics. Moreover, it has high cations exchange capacity, layered structure, large surface area, chemical, mechanical, and thermal stability. Surface modification of Bentonite using tunable molecular components enhances their removal capacity [9]. Polyoxometalates-Ionic Liquids (POM-ILs) as discrete transition metal-oxo anions and bulky organic are typical molecular components having tunable structure and offer several properties required for water decontamination [10]. Polyoxometalates (POMs) are huge class of inorganic nano sized metal-oxo cluster anions of the general formula $[MxOy]^{n-}$, composed of high-

valent transition metal (M) (M = W, V, Mo, Nb) in their highest oxidation state (d^0, d^1) linked together via oxo (O^{2-}) ligands [11]. Among various structural classes, Keggin-type polyoxometalates have acid–base and redox properties, and ease of preparation making them to receive considerable attention [12]. In a previous work, we prepared POMIL supported on Saudi bentonite TOAx[α-$XW_{11}O_{39}$]@Bentonite (X = Si, P; TOA = TetraOctylAmmonium) and investigated its removal of cationic dye from water [13].

This work aims to the preparation and characterization of $Q^8(PV_3W_9)$@B composite for the removal of MB from aqueous solutions. In addition to the examination of the effect of different parameters on the adsorption of MB. Kinetic, Isotherm and thermodynamic parameters were studied in order to evaluate the adsorption process of MB dye form wastewater. Investigation of the re-usability of adsorbent and antibacterial activity were also performed.

2. Materials and Methods

2.1. Materials

Bentonite was collected from Khulays bentonite deposit in Saudi Arabia. All reagents used were analytical grade and were not subjected to additional purification. Analytical grade Methylene Blue (MB) ($C_{16}H_{18}ClN_3S$), supplied from Fluka was used without further purification. Sodium tungstate Na_2WO_4, Ammonium vanadate(V) (NH_4VO_3) and sodium acetate (CH_3COONa) were all obtained from J.T. Baker. Distilled water was used to prepare all aqueous solutions in the study.

2.2. Adsorbent Preparation

The adsorbent preparation was performed according to three steps. First Keggin-type polyoxometalates preparation was synthesized using the same procedure as in inorganic synthesis [10]. Then preparation of polyoxometalate Ionic liquid POM-IL by metathesis reaction, followed by impregnation of the Bentonite.

2.2.1. Synthesis of $Na_9[A\text{-}PW_9O_{34}]$

Sodium nonatungstate was synthesized using the same procedure as in inorganic synthesis [10] A mixture of 60 g (0.18 mol) of sodium tungstate dihydrate $Na_2WO_4{\cdot}2H_2O$ and 75 ml of water is stirred in a 200 mL beaker with a magnetic stirring bar until the solid is completely dissolved. 2.4 mL (0.035 mol) of Phosphoric acid (85%) were added dropwise. After addition of the acid is complete, the measured pH is 8.9. 11.4 mL (0.19 mol) of glacial acetic acid is added dropwise with vigorous stirring. Large quantities of white precipitate form during the addition. The final pH of the solution is 7.6 ± 0.3. The solution is stirred for 1 h, and the precipitate is collected and dried by suction filtration on a medium frit.

2.2.2. Synthesis of $Q^8PV_3W_9O_{40}$

In 250 mL beaker, 8.2 g (0.1 mol) of sodium acetate were dissolved in 100 mL of distilled water at Room Temperature (R.T). The pH of the solution was adjusted to 4.8 by adding approximately 3.5 mL (0.06 mol) of acetic acid. To this solution

2.9 g (0.024 mol) of NH_4VO_3 were added under vigorous stirring, then 20 g (0.0082 mol) of $Na_9[A\text{-}PW_9O_{34}]$ were added and stirred for 48 h at R.T. The wine-red solution was filtered by suction frit porosity 4 to remove unreacted orange solid. Afterwards 13.4 g (0.024 mol) of tetraoctylammonium bromide in 50 mL of toluene were added to the solution. The reaction mixture was started to separate into two layers after addition of 50 mL of toluene. In the biphasic system the organic layer turned dark red after shaking in the separation funnel. The organic phase was separated, and the solvent removed under vacuum by rotary evaporator.

2.2.3. Synthesis of $Q^8PV_3W_9$@B

1.16 g of $Q^8PV_3W_9$ (0.002 mol), was dissolved in 50 mL of acetone and then 4.5 g of Bentonite were added. The suspension was gently shaken for 30 min and the solvent was removed by rotary evaporator. 50 mL of acetone was added, and impregnation procedure was repeated four times. The final product $Q^8PV_3W_9$@B was obtained as a solid, free flowing powder.

2.3. Characterizations of Adsorbent

Information regarding the crystalline structures was obtained through X-ray diffraction (XRD) analysis using a powder PXRD diffractometer (Model Equinox 1000-INEL, France) with Co Kα radiation (λ = 1.7890 Å) at 30 kV and 30 mA. The polyoxometalates (POMs) were compared to the parent Keggin structure using reference data from the International Centre for Diffraction Data (ICDD) database. Sample morphology was examined using field emission scanning electron microscopy (FEG-SEM) with a Quanta FEG450 (FEI, Netherlands). This involved an ETD Everhart Thornley detector in High Vacuum mode, a solid-state backscattering electron detector (VCD), and an EDS detector (XFLASH6-30, Bruker) to determine the elemental composition of the samples. The dispersion and size of POM particles on the Bentonite support, as well as the layered structure of Bentonite and POM-IL@Bentonite, were confirmed using transmission electron microscopy (TEM) with a Tecnai G2 F20 Super Twin (FEI, Netherlands) equipped with a LaB6 source operating at 200 kV. The electron microscope also had an EDS detector for elemental analysis. Nanoprobe scanning transmission electron microscopy (STEM) imaging was conducted with a HADAF detector, and TEM images were captured using a Gatan camera at 200 kV with 2k × 2k resolution. Data from TEM, high-resolution TEM (HRTEM), STEM, and EDS were collected and processed using TIA software (Tecnai Imaging and Analysis version 1.9.162) and Gatan Micrograph Software version 2.3.

The surface functional groups of POM-IL and Bentonite were analyzed using Fourier transform infrared spectroscopy (FTIR) with a Bruker Tensor II spectrometer. Nitrogen sorption analysis was performed to evaluate the specific surface area (using the BET method), specific pore volume, and pore diameter (using the BJH method) of both raw and POM-SIL modified bentonite, utilizing a NOVA (2200 e) high-speed surface area and pore size analyzer.

2.4. Preparation of Adsorbate

Analytical grade Methylene Blue (MB) and used without further purification. The chemical structure of MB is shown in Figure 1. Stock solution of 1000 ppm, was prepared by dissolving a 1g of MB in 1 L of distilled water. The experimental solution was prepared by using distilled water for diluting the stock solution. The concentration of Methylene Blue dye before and after adsorption were determined using UV spectrophotometer, GENESYS 10S UV-VIS. As can see in Figure 1, the absorption spectrum of the Methylene Blue is characterized by three main bands, one in the visible region (λ_{max}= 665 nm), and two in the UV region (λ_{max} = 292 nm and λ_{max} = 246 nm). In our case, the most important band is at 665 nm.

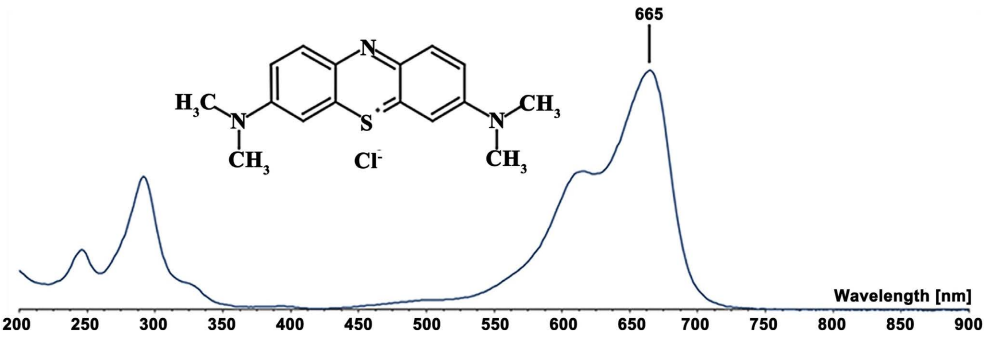

Figure 1. Absorbance of methylene blue (MB) at λ_{max} = 665 nm (C = 5 mg/L).

2.5. Adsorption Experiment

2.5.1. Batch Method

Adsorption test for the dye removal from aqueous solution was conducted using adsorption batch experiments to explore the adsorption properties and the factors influencing the adsorption. Batch experiments were performed by varying contact time, mass of adsorbents, concentration of dyes, pH and temperature. The following conditions were preserved for the different sets of experiments:

1) The effect of pH was conducted in the range from 2.0 to 12, 100 mg of $Q^8PV_3W_9$@B and, 100 mL solution volume, 50 ppm MB concentration and T = 298 K. HCl (0.01 M) or NaOH (0.01 M) was added to set the desired pH value.

2) Effect of contact time was carried out through the time intervals (10, 20, 30, 40, 50, and 60 min), 100 mg of adsorbent, 100 mL solution, 50 ppm MB concentration, 298 K, initial non modified pH.

3) The effect of adsorbent mass was examined using different doses (20, 40, 60, 80 and 100 mg) of adsorbent, initial non modified pH, time 60 min, 50 ppm MB concentration, 100 mL solution volume, and temperature 298 K.

4) The effect of initial concentration was conducted using 40, 50, 60, 100, 200, 300, 400, 500 mg/L of MB, initial non modified pH, time 60 min, adsorbent mass 100 mg of $Q^8PV_3W_9$@B and temperature 298 K.

5) The influence of temperature on the adsorption process was studied under different temperatures of 298, 303, 308, 313 and 318 K, initial non modified pH, time 60 min, 50 mg/L MB concentration, adsorbent mass 20 mg, solution volume

100 mL.

In each Experiment, the adsorbent is stirred at 300 rpm in the MB solution until the adsorption is reached. After that, the dye residual concentration is measured. After adsorption the dye was kept apart from the adsorbent by centrifugation with 3000 rpm speed and use UV-VIS spectrophotometric technique to determine the C based on Beer-lambert equation.

2.5.2. Data Processing

The amount of the dye adsorbed per unit mass; Q_t will be calculated using the equation

$$Q_t = \frac{C_0 - C_f}{m} \times V \tag{1}$$

And the Removal efficiency: (R%)

$$R\% = \frac{C_0 - C_f}{C_0} \times 100 \tag{2}$$

where C_0 and C_f (mg·L^{-1}) are the initial and final MB concentration, V (mL): the dye solution volume, m (mg): the adsorbent mass.

2.6. Reusability Test

The reusability of the adsorbent makes it prominent adsorbent material for the adsorption and make it more economical. Adsorbents obtained after adsorption experiments were dried at (120˚C) and then shaken in 30 mL of ethanol for 15 min twice to remove the adsorbed dye. After that 400 mL of distilled water were added and the suspension was stirred under 80˚C in order to achieve desorption.

2.7. Antibacterial Activity

Antimicrobial activities of the $Q^8PV_3W_9$ and $Q^8PV_3W_9$@B were performed against two different pathogenic bacteria gram-positive bacteria: S. aureus ATCCBAA977 and gram negative bacteria E. coli ATCC25922. The bacterial inoculum concentration (6×10^6 CFU/ml) uniformly spread using a sterile cotton swab on a sterile Petri dish containing Muller–Hinton agar medium [11] [12]. For this, the discs were placed on Petri plates containing bacterial culture was poured in pores 0.1 ml $Q^8PV_3W_9$ and $Q^8PV_3W_9$@B (9 mm in diameter) in Muller–Hinton agar medium. The plates incubated for 24 h at 37˚C ± 1˚C, under aerobic conditions. After incubation, confluent bacterial growth was observed. Inhibition of bacterial growth was measured in mm.

3. Results and Discussion

3.1. Characterization of $Q^8PV_3W_9$@B

3.1.1. Fourier Transform Infrared (FTIR)

The FTIR spectra of raw Bentonite, $Q^8PV_3W_9$@B in the range of 4000 - 400 cm^{-1} were shown in **Figure 2**. FT-IR spectrum of the $Q^8PV_3W_9$@B showed that in the low frequency region, the modified and unmodified Bentonites are largely

comparable indicating that the clay mineral has not changed upon addition of $Q^8PV_3W_9$ to Bentonite. Besides, no peak shift was observed during the modification which indicates the retention of the structure of Bentonite.

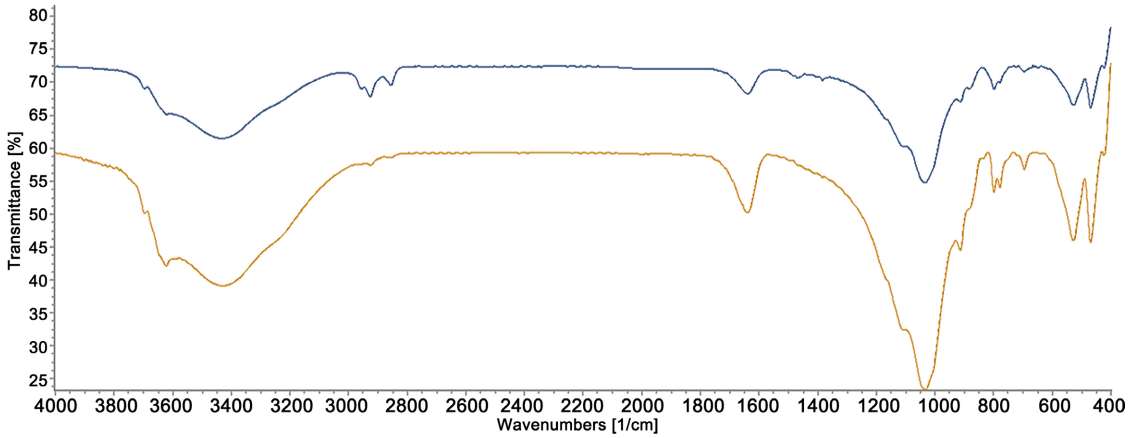

Figure 2. Infrared spectra (from top to bottom) of Bentonite and $Q^8PV_3W_9$@B.

The absorbance peaks at 524 cm^{-1}, 914 cm^{-1} and 468 cm^{-1} ascribed respectively to δ(Al-O-Si), δ(Al-Al-OH), δ(Si-O-Si) which confirm the presence of montmorillonite.

The very strong characteristic peak observed at 1032 cm^{-1} was ascribed to asymmetric stretching vibrations of Si-O-Si bonds. The broad band in the 3430 - 3623 cm^{-1} region can be ascribed to the symmetric stretching of (Si-OH, Al-OH) structural hydroxyl groups OH and of the physically adsorbed water OH. The shoulder at 3694 cm^{-1} and the weak band at 695 cm^{-1} suggest the presence of kaolinite. The absorption band at 1639 cm^{-1} is attributed to the angular vibration of the OH group and related to the adsorbed water and the hydration water present in the clay.

The presence of tetraalkylammonium cation is confirmed by the presence of peaks at 1379 and 1460 cm^{-1} which are assigned to C-H scissoring vibrations of CH_2-N^+ and peaks at 2855 and 2956 cm^{-1} assigned to the symmetric and asymmetric stretching modes of -CH_2 of organic cation [14].

The characteristic bands for POM are not observed in low frequency, they overlaped with the characteristic band of Bentonite.

3.1.2. Scanning Electron Microscope Analysis (SEM)

The SEM results for the raw Bentonite sample presented in **Figure 3(A)**. As can be seen, raw Bentonite has a rough surface with large number of pores distinguished as dark areas. SEM images in **Figure 3(B)** for modified Bentonite by POM-IL samples show that chemical modification by $Q^8PV_3W_9$ lead to a change of the surface morphology of raw Bentonite and presents rose-like agglomerates on the surface.

After loading with MB dye molecules, the morphology has changed and becomes cloudy, the layered-stacking structure is no more observed. This change is

due to the occupation of MB molecules into the heterogeneous pores of $Q^8PV_3W_9$ @B as shown in Figure 3(C) [15].

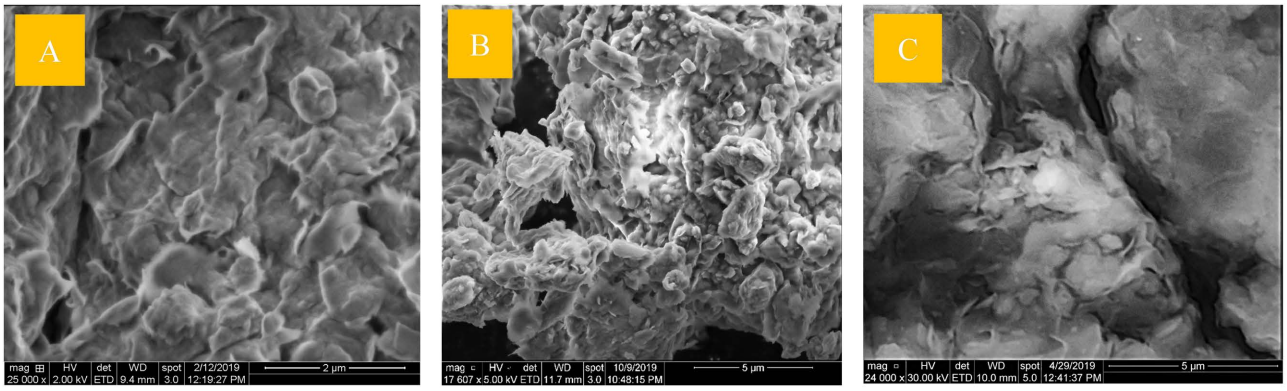

Figure 3. (A) SEM images for raw Bentonite, (B) $Q^8PV_3W_9$@B and (C) MB-$Q^8PV_3W_9$@B.

3.1.3. Chemical Composition

EDS analysis in Table 2 showed that natural Saudi bentonite is mainly composed of silicon dioxide, Aluminum oxide, iron oxide, sodium oxide, in addition to calcium, magnesium, titanium and potassium oxides. Figure 4 revealed appearance of new peaks of P, W, V relative to PV_3W_9 polyoxometalate with the correct V/W ratio (3:9); this result confirms that PV_3W_9 is present in the prepared adsorbent and retain its keggin structure.

Table 2. Chemical composition of raw Saudi bentonite and POM-IL modified bentonite.

Main constituent	SiO_2	Al_2O_3	Fe_2O_3	MgO	TiO_2	Na_2O	CaO	K_2O
Raw Bentonite wt%	5.38	22.71	6.25	3.02	1.35	2.78	1.64	0.55
$Q^8PV_3W_9$@B	52.16	23.25	6.59	3.33	1.08	2.98	1.57	0.75

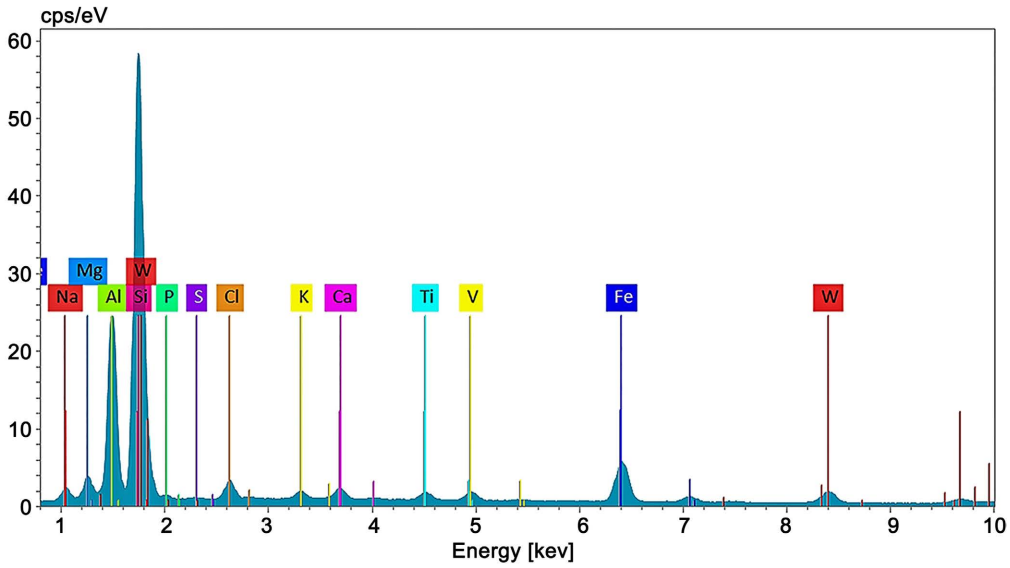

Figure 4. EDS of $Q_6^8PV_3$@B.

3.1.4. Powder X-Ray Diffraction (PXRD)

The X-ray patterns of raw Bentonite, $Q^8PV_3W_9$@B. are illustrated in Figure 5.

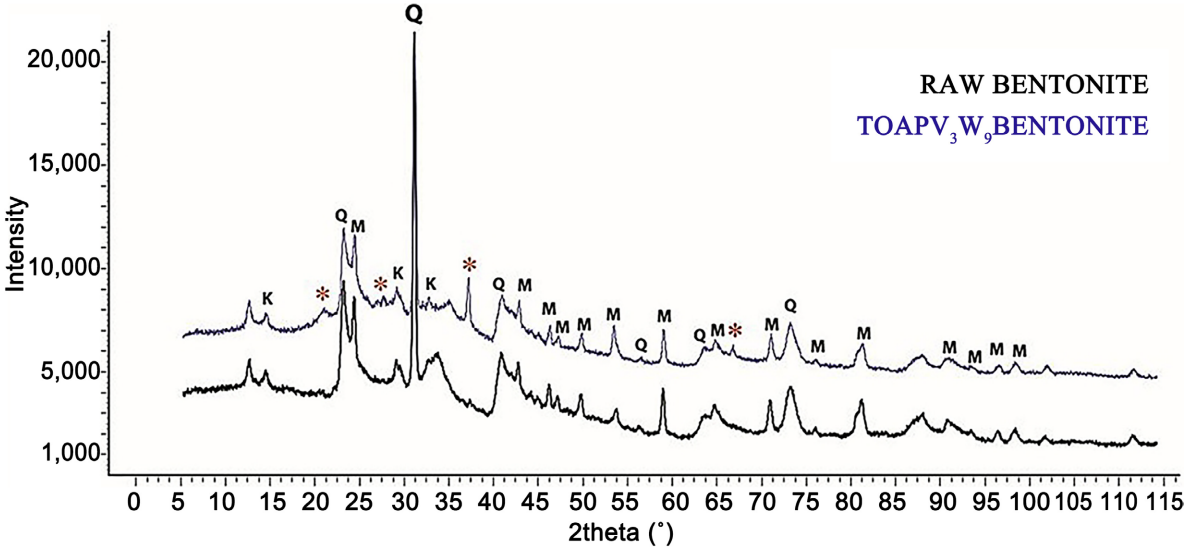

Figure 5. XRD analysis for $Q_6^8PV_3$@B and Raw Bentonite (2θ: 0˚ to 120˚).

The XRD pattern of raw Bentonite in Figure 5 shows the presence of montmorillonite (6.26˚, 24.30˚, 42.67˚, 46.12˚, 49.57˚, 53.54˚, 58.88˚) as major phase. The results show that the characteristic peaks of the Bentonite support are not affected during the POM impregnation with Bentonite.

The X-ray diffractometer recorded in a range of small angle (2θ) ranging from 0˚ to 10˚ shows the presence of a characteristic diffraction peak located at $2\theta = 6$˚ from which the interlayer distance was found to be 14.08 Å. This peak is associated with the (001) diffraction (d001) of the montmorillonite phase [16].

The introduction of POM to the Bentonite does not affect the d001 diffraction peak which appears at 14.75 Å for $Q^8PV_3W_9$@B (Figure 6). This finding confirmed that the structure of Bentonite is retained after impregnation by $Q^8PV_3W_9$@B.

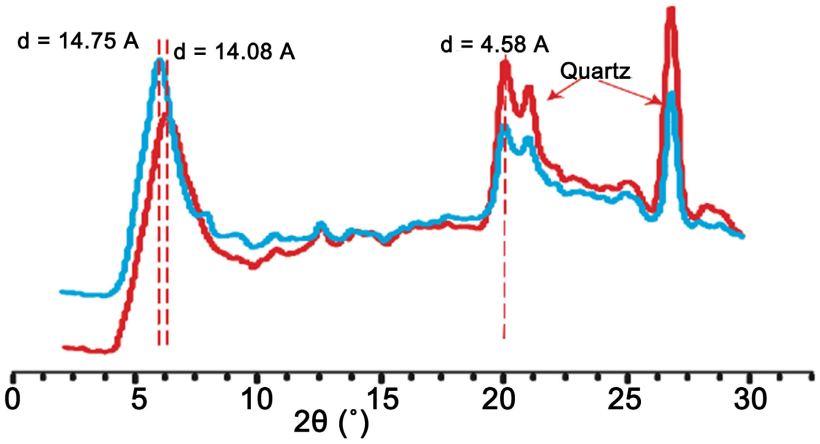

Figure 6. XRD analysis of $Q^8PV_3W_9$@B (blue) and Raw Bentonite (red) at low angle (2θ: 0 to 30˚).

Moreover, the presence of POM in the prepared adsorbent is confirmed by the presence of structural characteristic peaks in the ranges of 2θ (5˚ - 10˚, 17˚ - 22˚, 25˚ - 30˚, and 31˚ - 37˚) in agreement with the Keggin structure [17] [18].

3.1.5. Transmission Electron Microscopy Analysis (TEM)

TEM characterization carried out on the POM modified Bentonite are presented in Figure 7. TEM analysis confirmed the XRD results and revealed the existence of layers at basal space d_{001} = 14.08 A for Bentonite and d_{001} = 14.75 A for POM modified Bentonite. There is no significant expansion of interlayer space θd (4.38 A and 5.05 A).

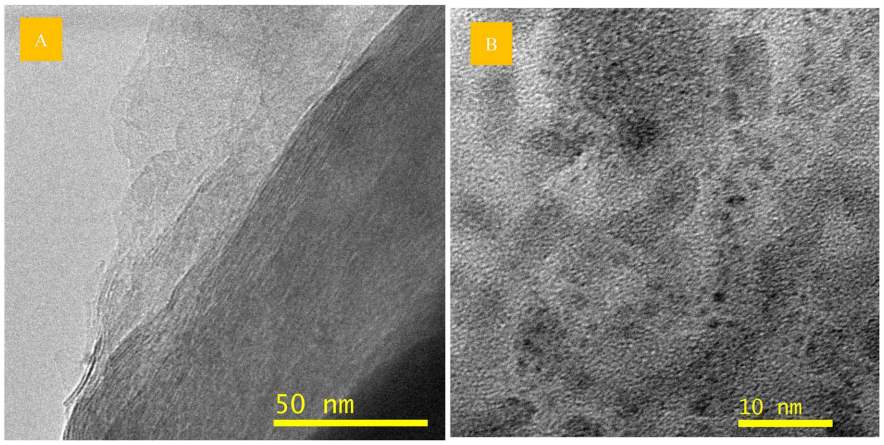

Figure 7. TEM images of $Q^8PV_3W_9$@B.

3.1.6. Nitrogen Sorption Analysis

Nitrogen sorption was used to investigate the specific surface area (BET method), specific pore volume and pore diameter (BJH method) of the Raw Bentonite and $Q^8PV_3W_9$@B to establish the consequences of POM-IL adsorption on the Bentonite pore structure. The data in Table 3 show that an overall reduction in pore diameter, specific pore volume and specific surface area is observed, with respect to the raw bentonite reference, indicating that the $Q^8PV_3W_9$ coats the exterior surface and some of the internal pore structure.

Table 3. BET results for raw bentonite and $Q^8PV_3W_9$@B.

Parameter	adsorbents	
	Raw Bentonite	$Q^8PV_3W_9$@B
Specific surface area	59.4 m^2/g	1.16 m^2/g
Specific pore volume	0.0695 cm^3/g	0.0647 cm^3/g
pore diameter	3.52 nm	2.96 nm

3.2. MB Adsorption Experiments

3.2.1. Effect of Contact Time

The effect of contact time on Methylene Blue removal by $Q^8PV_3W_9$@B is shown in Figure 8. It could be seen that the percentage removal increase with increasing

the contact time, and occurred in two stages: first fast stage and equilibrium stage. The uptake is rapid for the first stage (5 min) with 48.2% removal. This fast kinetic is due to the presence of high number of available vacant sites. The equilibrium was reached within almost 20 min with total removal. Futher increase in contact time will no longer improve the percentage removal.

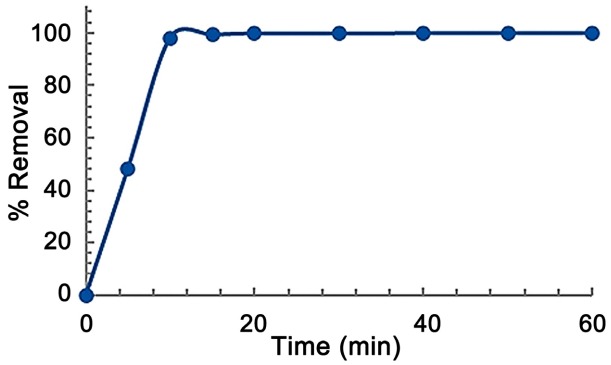

Figure 8. Effect of contact time on the adsorption of MB using $Q^8PV_3W_9$@B.

3.2.2. Effect of Adsorbent Mass

The percentage removal of dye is directly proportional to the adsorbent mass. As seen clearly from **Figure 9** $Q^8PV_3W_9$@B the adsorbent mass used, ranged from (20 - 100 mg). As expected, the results followed the general trend with adsorbent mass. In fact, The findings revealed that the percentage of adsorption of Methylene Blue dye increased with increasing amount of the modified Bentonite from 37.2% (20 mg) to 100% (100 mg); this might have been ascribed to an enhanced surface area of the adsorbent and the availability of additional adsorption sites.

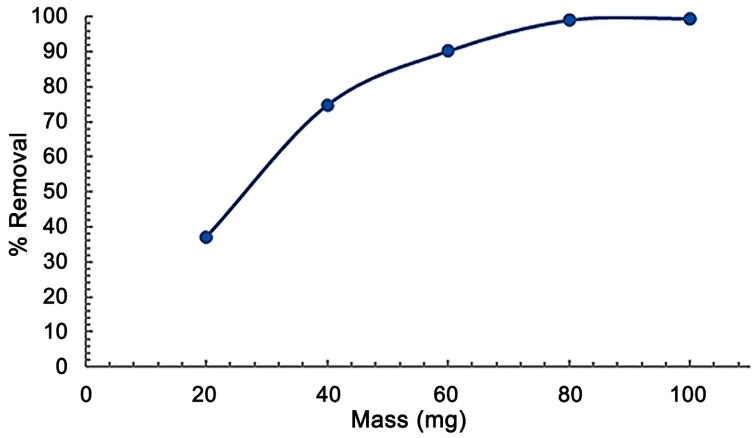

Figure 9. Effect of adsorbent mass on the adsorption of MB using $Q^8PV_3W_9$@B.

3.2.3. Effect of Concentration

Methylene blue dye solution of different concentration ranging from 50 - 500 mg/L were prepared by dilution from the 1000 ppm stock solution. The effect of initial concentration on the removal of methylene blue on $Q^8PV_3W_9$@B is shown in **Figure 10**.

The results show that the % removal of MB increased initially and reached more than 95% with concentration of (50 - 200 mg/L) at constant adsorbent amount (100 mg). Adding more methylene blue above the saturation level (200 mg/L) did not find available vacant sites resulting on the formation of accumulation of methylene blue molecule on the surface of adsorbent and the percentage removal decrease.

The adsorption capacity (Q_e) increased gradually with the increase in concentration Figure 10(A). However, at lower dye concentrations, the adsorption is independent of initial concentration since the ratio of the number of MB cations to the number of available adsorption sites is small.

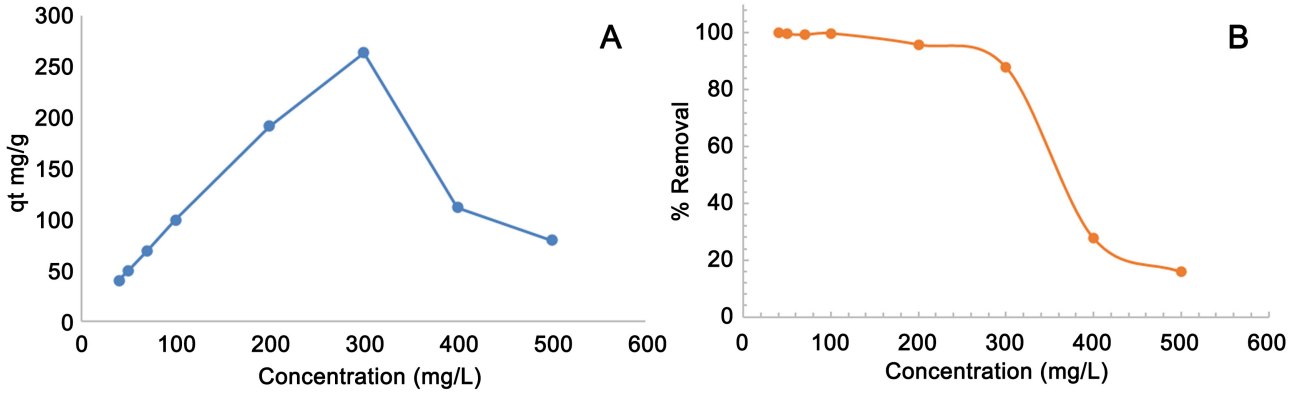

Figure 10. Effect of initial concentration on the adsorption of MB using $Q^8PV_3W_9$@B.

3.2.4. Effect of pH

The pH experiments were performed at pH ranging from 2 to 12. According to reported studies on the adsorption of dye, the effect of pH on the solute adsorption capacity and removal by c can be slightly or moderately significant.

For MB dye used in this study, the result related to the pH dependence are apparently surprising.

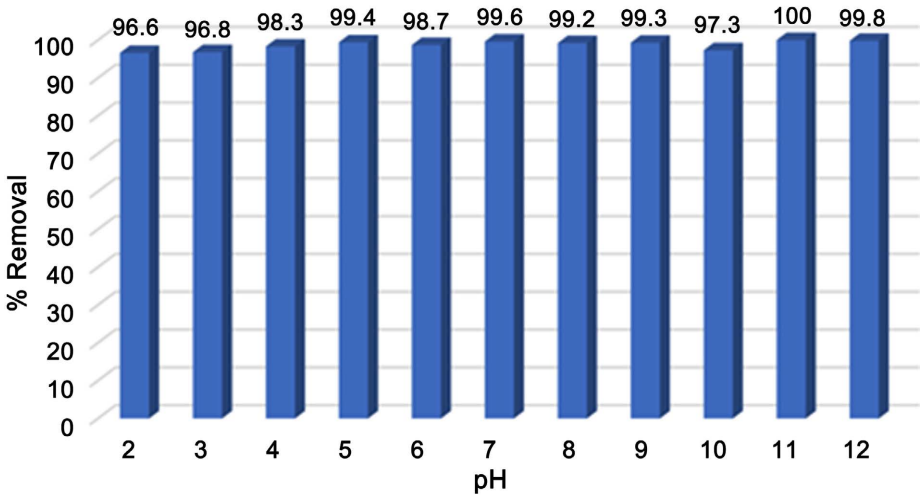

Figure 11. Effect of pH on the adsorption of MB using $Q^8PV_3W_9$@B.

As shown in Figure 11 there is no significant effect on the adsorption of methylene blue while changing the pH solutions values, $Q^8PV_3W_9$@B is stable adsorbent over a wide pH range [19] [20].

Independent of the origin of this insignificant effect of the pH, this finding is quite meaningful in the adsorption process application since it makes pH adjustment of the effluent before treatment unnecessary. Since pH control is complicated and difficult to realize.

As a result, pH will not be adjusted during adsorption experiment to simulate real treatment condition of industrial effluents.

3.2.5. Effect of Temperature

The experimental results are shown in Figure 12. The influence of temperature on the adsorption of MB onto $Q^8PV_3W_9$@B was carried out at 5 different temperatures ranging from 298 to 318K. Figure 12 shows that the removal percentage of MB increased with the increase in temperature; indicating that the adsorption process of methylene blue dye is endothermic in nature. The increase of adsorption is due to the absorbed heat used as activation energy.

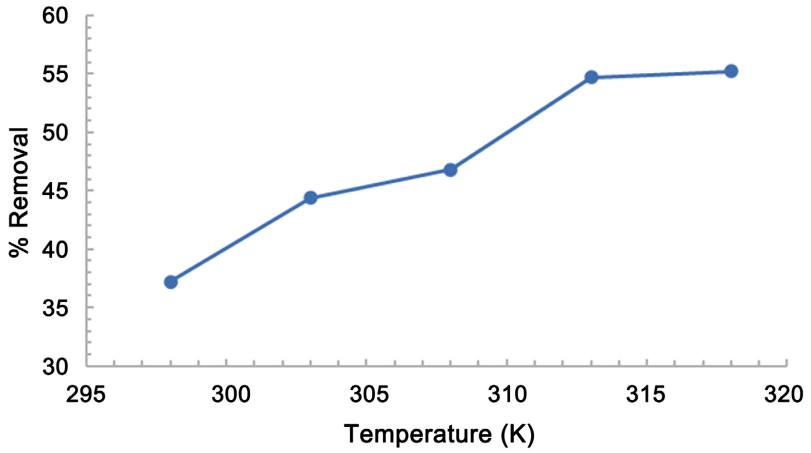

Figure 12. Effect of temperature on the adsorption of MB using $Q^8PV_3W_9$@B.

3.3. Kinetic Study

Lagergren's first order, Ho's second order kinetic and the intraparticle diffusion model are applied in this study to determine the rate of adsorption at different time intervals.

3.3.1. Lagergren Pseudo First Order

Lagergren [21], proposed the first order kinetics and improved and was given by

$$\ln\left(q_e - q_t\right) = \ln q_e - K_1 t \tag{3}$$

where q_e and q_t are amounts of dye adsorbed (mg/g) per unit mass at equilibrium and at any time t (min), K_1 is the first order constant.

3.3.2. Pseudo-Second Order

The pseudo second-order rate equation by Ho [22], can be expressed as follows:

$$\frac{t}{q_t} = \frac{1}{K_2 q_e^2} + \frac{1}{q_e} t \tag{4}$$

where q_e and q_t are amounts of dye adsorbed (mg/g) at time t (min) at equilibrium and at any time t respectively, K_2 is the second order constant.

The kinetics of MB dye adsorption onto $Q^8PV_3W_9$@B were analyzed using pseudo-first-order PFO model (Equation (3)) and pseudo-second order PSO model (Equation (4)).

It was found that pseudo-first-order kinetic model did not well fit. Plot of $\ln(q_e - q_t)$ vs. t is not linear.

On other hand, the plot of t/q_t vs. t for pseudo-second-order model (**Figure 13**) is applicable over the whole range of contact time with excellent linearity.

The kinetic parameter for pseudo-first-order and pseudo-second order were calculated and tabulated in **Table 4**.

Table 4. Kinetic parameters for PFO and PSO models.

Parameter	Kinetic Model	
	1st order	2nd order
$Q_{e,cal}$ (mg/g)	1.79	51.5
K	0.0797 (min^{-1})	0.0128 (g/mg min)
R^2	0.5231	0.9935
$Q_{e,exp}$ (mg/g)	49.9	

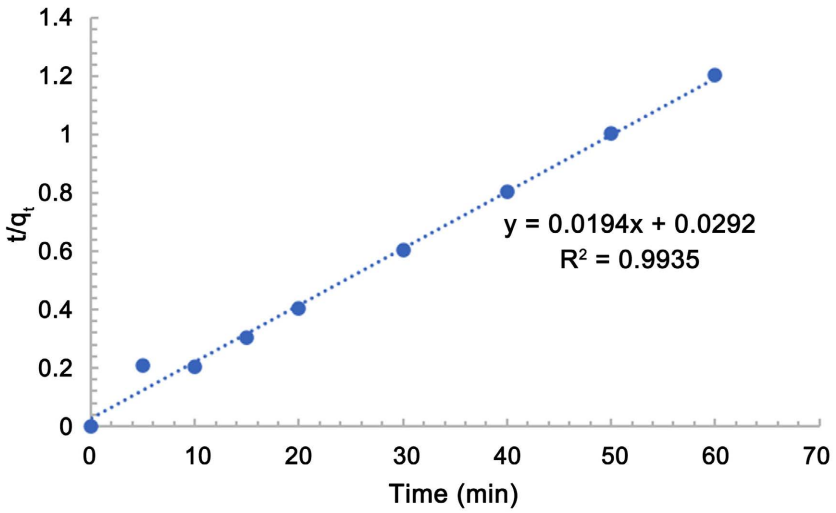

Figure 13. Pseudo second order plot for adsorption of MB onto 100 mg of $Q^8PV_3W_9$@B.

The real test for the validity of the kinetic model arises from the comparison between the experimentally determined ($q_{e,exp}$) and the calculated ($q_{e,cal}$) [21] [22].

It can be noticed that in the pseudo-second-order kinetic model, the calculated q_e (51.5 mg/g) is very close to the experimental q_e (49.9 mg/g). In addition, the

correlation coefficient R^2 for the pseudo-second-order ($R^2 = 0.9935$) is higher than that obtained for pseudo-first-order ($R^2 = 0.5231$).

Therefore, it is reasonable to conclude that the pseudo-second-order model is the obeyed model.

3.4. Equilibrium Study: Adsorption Isotherm

The adsorption isotherm is important for the description of how the adsorbate will interact with the adsorbent and give an idea about the adsorption capacity of the adsorbent. In this study Langmuir, Freundlich isotherm models were used to evaluate the equilibrium experimental data.

3.4.1. Langmuir Isotherm

Langmuir isotherm predicts the formation of adsorbed solute monolayer and is based on the assumption that dye molecules are adsorbed on a fixed number of well-defined sites, each site con hold a unique molecule [23]. The general equation for Langmuir is:

$$q_e = \frac{q_{\max} K_L C_e}{1 + K_L C_e} \tag{5}$$

where, q_e is the dye adsorbed amount at equilibrium (mg/g). $q_{\max}$ is the maximum adsorption capacity (mg/g). K_L is the constant for Langmuir. C_e is dye concentration at equilibrium.

Langmuir model can be mathematically expressed as:

$$\frac{C_e}{q_e} = \frac{1}{q_{\max} K_L} + \frac{C_e}{q_{\max}} \tag{6}$$

The value of $(1/q_{\max})$ and K_L can be obtained from linear curve of (C_e/q_e) versus C_e, R_L provide information about the affinity between adsorbate and adsorbent which can be calculated using the following equation:

$$R_L = \frac{1}{1 + K_L C_o} \tag{7}$$

where K_L is the Langmuir constant. C_o (mg/L) is the initial concentration of dye.

The R_L separation factor values (Table 5) indicate the nature of the adsorption to be:

Table 5. The R_L values indicate the nature of the adsorption.

R_L	($R_L = 0$)	($0 < R_L < 1$)	($R_L = 1$)	($R_L > 1$)
Type of isotherm	irreversible	favorable	linear	unfavourable

3.4.2. Freundlich Isotherm

The Freundlich equation is empirical and represent the equilibrium on heterogeneous surfaces.

The Freundlich model in its linear form is express as:

$$q_e = K_f \left(C_e\right)^{1/n} \tag{8}$$

where C_e is the equilibrium dye concentration (mg/L), q_e is the dye adsorbed amount at equilibrium (mg/g). K_f are the Freundlich constants and n indicative of the extent of the adsorption and the degree of nonlinearity between solution concentration and adsorption intensity.

The Freundlich equation can also be linearized in logarithmic form as shown below:

$$\log q_e = \log K_f + \frac{1}{n}\log C_e \tag{9}$$

where C_e is the equilibrium concentration (mg/L). q_e is the adsorbed amount at equilibrium (mg/g). K_f and n are Freundlich coefficients, related respectively to adsorption capacity and adsorption intensity of the solid adsorbent.

The slope and the intercept of the plot $\log q_e$ Vs $\log C_e$ correspond to $(1/n)$ and $\log K_f$, respectively.

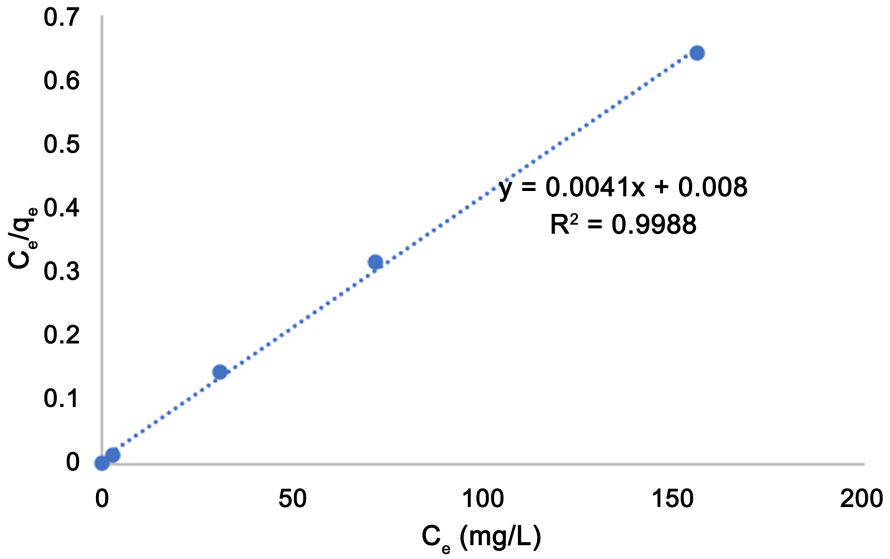

Figure 14. Langmuir isotherm plot for adsorption of MB onto $Q^8PV_3W_9$@B.

Table 6. Isotherm adsorption study equation parameter of the MB on $Q^8PV_3W_9$@B.

Isotherm	Parameter	$Q^8PV_3W_9$@B
Langmuir	Q_{max} (mg/g)	243.90
	K_L (L/mg)	0.51
	R^2	0.9988
Freundlich	n (g/L)	28.3286
	K_f (mg/g)	192.71
	R^2	0.6737

Figure 14 and Table 6 summarize the calculated coefficients of determination (R^2) and model parameters of the Langmuir and Freundlich isotherms. The results show clearly that the experimental data fit better to the Langmuir isotherm model

(R^2 = 0.9495) than Freundlich (R^2 = 0.7251) which indicates homogeneous and monolayer coverage of MB cations at the surface of the $Q^8PV_3W_9$@B. The maximum adsorption capacity for MB onto $Q^8PV_3W_9$@B was 270 mg/g. Moreover, the adsorption is considered favorable when the separation factor R_L equation (7) range between 0 and 1 as shown in **Table 5** [24].

The R_L values for MB for each initial concentration was greater than zero and less than unity which indicates favorable adsorption.

Moreover, it is observed that R_L values are decreasing with increasing initial concentration which implies that the adsorption of MB becomes more favorable.

3.5. Thermodynamic Parameters

In order to evaluate the effect of temperature on the adsorption process and the thermodynamic function. ΔG° The standard Gibbs free energy, the standard ΔH° enthalpy, were calculated using the below Equations:

$$\Delta G^\circ = -RT \ln K_{dc} \tag{10}$$

$$\ln K_{dc} = -\frac{\Delta H^\circ}{RT} + \frac{\Delta S^\circ}{R} \tag{11}$$

$$K_{dc} = \frac{q_t}{C_t} \tag{12}$$

The standard entropy values (J/mol·K), ΔS°, were calculated by use Gibbs–Helmholtz equation as follows:

$$\Delta S^0 = \frac{\Delta H^0 - \Delta G^0}{T} \tag{13}$$

where K_{dc} (Lg^{-1}) is Distribution coefficient, T (K): temperature expressed in Kelvin.

R is Gas constant (8.314 $J{\cdot}mol^{-1}{\cdot}K^{-1}$).

Table 7. Thermodynamic parameters of the MB on $Q^8PV_3W_9$@B.

adsorbent	T (K)	ΔG° (J/mol)	ΔS° ($J.K^{-1}mol^{-1}$)	ΔH° (J/mol)
$Q^8PV_3W_9$@B	298	−2688.78	108.52	29650.81
	303	−3488.68	109.37	
	308	−3793.01	108.58	
	313	−4681.08	109.68	
	318	−4802.70	108.34	

Thermodynamic parameters of the MB dye on $Q^8PV_3W_9$@B are summarized in **Table 7**. It is obvious that at higher temperatures the adsorption of MB onto $Q_6{}^8$PV3@B was favorable. The ΔG° values are negative at all temperatures become more negative with increasing temperatures indicating the adsorption process is spontaneous. Mainly owing to chemisorption rather than physisorption [25]. The value of standard enthalpy change was positive ($\Delta H^\circ > 0$), showing that adsorption is of MB an endothermic process. The positive values of ΔS° indicate that the MB dye adsorption process increase the randomness at the solid-liquid

interface during the adsorption process and suggest a strong affinity between MB and $Q_6^8PV_3$@B [26].

Reusability Test

The ability of the adsorbents to be reused is a crucial factor. Reusability of the adsorbent is usually carried out in order to avoid the cost of a new acquisition and minimizing the amount of waste. In order to evaluate the reusability of adsorbents, ethanol was selected as elution solvent. The recycled adsorbent indicated reasonable efficiency (100%) after eleven consecutive cycles as shown in Figure 15. These results revealed that the Q^8PV_3 W_9@B have a good potential as cost-effective adsorbent for removal.

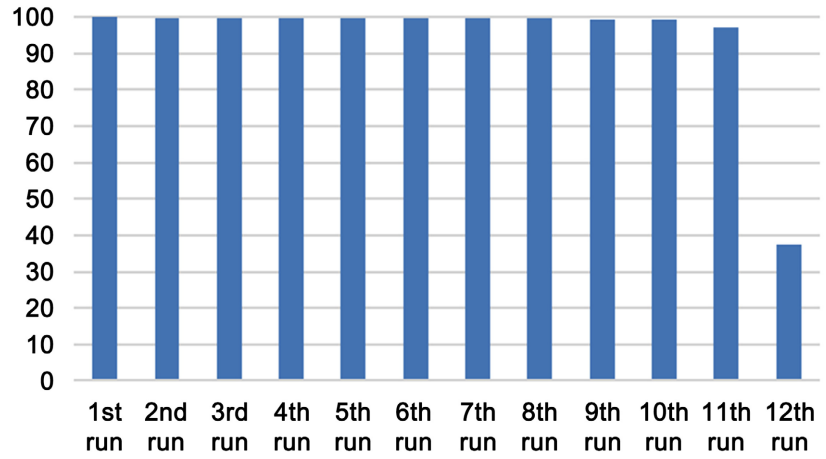

Figure 15. Reusability test for adsorbent (Q^8PV_3 W_9@B).

3.6. Evaluation of Antibacterial Activity

Antibacterial activity is considered as an important criterion for the evaluation of adsorbent features in water decontamination. The antibacterial activity of Free Bentonie and $Q^8PV_3W_9$@B against different bacterial isolates was tested and showed a higher score in the case of gram negative than gram positive pathogenic bacteria. The antibacterial of free Bentonite and $Q^8PV_3W_9$@B is shown in Figure 16, against pathogenic *E. coli* ATCC25922 and *S. aureus* ATCCBAA977. Free Bentonie showed minor bacterial activity as illustrated in Figure 16(C), Figure 16(D), the bacteria

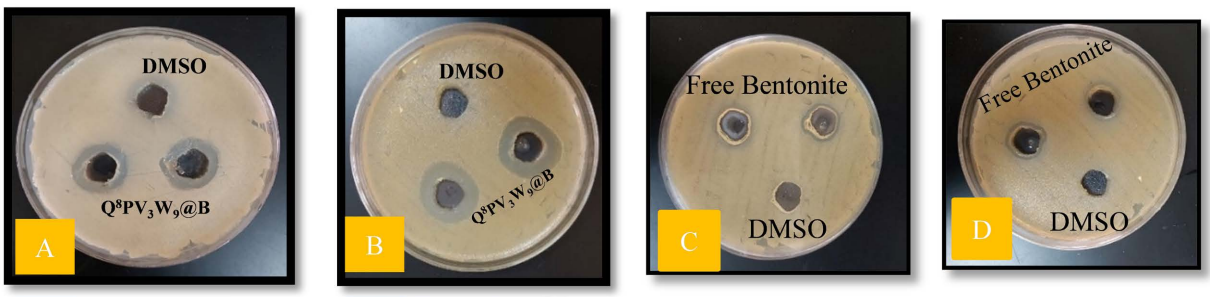

Figure 16. Inhibition test result for $Q^8PV_3W_9$@B and free Bentonite against two pathogenic bacteria (A) (C) *S. aureus* ATCCBAA977. (B) (D) *E. coli* ATCC25922.

was grown with no significant inhibitory zone. While, in case of $Q^8PV_3W_9$@B, the inhibtory zone was strong around the disc free of bacteria, showing an important antibacterial activity.

The incorpration of $Q^8PV_3W_9$ enhanced the antibacterial activity to the adsorbent. Similar result were reported in the case of $Q^x_8[\alpha\text{-}SiW_{11}O_{39}]$ $x = 6, 7$ supported on silica [27].

4. Conclusion

The new prepared $Q^8PV_3W_9$@B can be used as an inexpensive, reusable, and environment-friendly treatment option for MB contaminated water. The adsorption process was fast and attained equilibrium within 20 minutes. Kinetic study showed that the pseudo-second-order model described better the adsorption process suggesting the chemosorption nature of adsorption. Adsorption isotherms are described by the Langmuir model confirming the homogeneous monolayer coverage of the adsorbent. Overall, the adsorption process onto $Q^8PV_3W_9$@B was found to be spontaneous, endothermic and favorable. Moreover, $Q^8PV_3W_9$@B was tested for antibacterial activity against two different pathogenic bacteria gram-positive bacteria *S. aureus* ATCCBAA977 and gram-negative bacteria *E. coli* ATCC25922 and showed a higher score in the case of gram negative than gram positive pathogenic bacteria.

Conflicts of Interest

The authors declare no conflicts of interest regarding the publication of this paper.

References

[1] Malik, A.S., Boyko, O., Aktar, N. and Young, W.F. (2001) A Comparative Study of MR Imaging Profile of Titanium Pedicle Screws. *Acta Radiologica*, **42**, 291-293. https://doi.org/10.1080/028418501127346846

[2] Hu, T. and Desai, J.P. (2004) Soft-Tissue Material Properties under Large Deformation: Strain Rate Effect. *Proceedings of the* 26*th Annual International Conference of the IEEE EMBS*, San Francisco, 1-5 September 2004, 2758-2761. https://doi.org/10.1109/iembs.2004.1403789

[3] Ortega, R., Loria, A. and Kelly, R. (1995) A Semiglobally Stable Output Feedback Pi/Sup 2/D Regulator for Robot Manipulators. *IEEE Transactions on Automatic Control*, **40**, 1432-1436. https://doi.org/10.1109/9.402235

[4] Wit, E. and McClure, J. (2004) Statistics for Microarrays: Design, Analysis, and Inference. 5th Edition, John Wiley & Sons Ltd. https://doi.org/10.1002/0470011084

[5] Prasad, A.S. (1982) Clinical and Biochemical Spectrum of Zinc Deficiency in Human Subjects. In: Prasad, A.S., Ed., *Clinical, Biochemical and Nutritional Aspects of Trace Elements*, Alan R. Liss, Inc., 5-15.

[6] Giambastiani, B.M.S. (2007) Evoluzione Idrologica ed Idrogeologica Della Pineta di san Vitale (Ravenna). Ph.D. Thesis, Bologna University.

[7] Wu, J.K. (1994) Two Problems of Computer Mechanics Program System. In: *Proceedings of Finite Element Analysis and CAD*, Peking University Press, 9-15.

[8] Kennedy, K.K., Maseka, K.J. and Mbulo, M. (2018) Selected Adsorbents for Removal

of Contaminants from Wastewater: Towards Engineering Clay Minerals. *Open Journal of Applied Sciences*, **8**, 355-369. https://doi.org/10.4236/ojapps.2018.88027

[9] Wright and Wright, W. (1906) Flying-Machine. US Patent No. 821393.

[10] Ginsberg, A.P. (1990) Inorganic Syntheses. John Wiley & Sons, 27.

[11] Martín Caballero, J. (2017) Hybrid Polyoxometalates: Synthesis, Crystal Structures, Thermostructural Behavior and Anchoring to Tailored Polymeric Surfaces.

[12] Keggin, J. (1934) The Structure and Formula of 12-Phosphotungstic Acid. *Proceedings of the Royal Society of London. Series A, Containing Papers of a Mathematical and Physical Character*, **144**, 75-100. https://doi.org/10.1098/rspa.1934.0035

[13] Alsubaie, N., Alshamrani, R., Domyati, D., Alahmadi, N. and Bannani, F. (2021) Methylene Blue Dye Adsorption onto Polyoxometalate Ionic Liquid Supported on Bentonite: Kinetic, Equilibrium and Thermodynamic Studies. *Open Journal of Physical Chemistry*, **11**, 106-127. https://doi.org/10.4236/ojpc.2021.112006

[14] Abdalla, Z.E.A. and Li, B. (2012) Preparation of MCM-41 Supported $(Bu_4N)_4H_3(PW_{11}O_{39})$ Catalyst and Its Performance in Oxidative Desulfurization. *Chemical Engineering Journal*, **200**, 113-121. https://doi.org/10.1016/j.cej.2012.06.004

[15] Sabarinathan, C., Karuppasamy, P., Vijayakumar, C.T. and Arumuganathan, T. (2019) Development of Methylene Blue Removal Methodology by Adsorption Using Molecular Polyoxometalate: Kinetics, Thermodynamics and Mechanistic Study. *Microchemical Journal*, **146**, 315-326. https://doi.org/10.1016/j.microc.2019.01.015

[16] Eren, E. and Afsin, B. (2008) An Investigation of Cu(II) Adsorption by Raw and Acid-Activated Bentonite: A Combined Potentiometric, Thermodynamic, XRD, IR, DTA Study. *Journal of Hazardous Materials*, **151**, 682-691.

[17] Varadwaj, G.B.B. and Parida, K. (2013) Montmorillonite Supported Metal Nanoparticles: An Update on Syntheses and Applications. *RSC Advances*, **3**, 13583-13593.

[18] Tian, N., Zhu, M., Wu, Q., Yan, W. and Yaroslavtsev, A.B. (2014) Preparation and Conductivity of the Keggin-Type Trivanadium-Substituted Tungstosilicic Acid $H_7SiW_9V_3O_{40}{\cdot}9H_2O$. *Materials Letters*, **115**, 165-167. https://doi.org/10.1016/j.matlet.2013.10.052

[19] Jourvand, M., *et al.* (2015) Removal of Methylene Blue from Aqueous Solutions Using Modified Clay. *Journal of Basic Research in Medical Sciences*, **2**, 32-41.

[20] Nourmoradi, H., Nikaeen, M. and Khiadani (Hajian), M. (2012) Removal of Benzene, Toluene, Ethylbenzene and Xylene (BTEX) from Aqueous Solutions by Montmorillonite Modified with Nonionic Surfactant: Equilibrium, Kinetic and Thermodynamic Study. *Chemical Engineering Journal*, **191**, 341-348. https://doi.org/10.1016/j.cej.2012.03.029

[21] Lagergren, S.K. (1898) About the Theory of So-Called Adsorption of Soluble Substances. *Kungliga Svenska Vetenskapsakademiens Handlingar*, **24**, 1-39.

[22] Aksu, Z. and Tezer, S. (2005) Biosorption of Reactive Dyes on the Green Alga Chlorella Vulgaris. *Process Biochemistry*, **40**, 1347-1361. https://doi.org/10.1016/j.procbio.2004.06.007

[23] Liu, L., Luo, X., Ding, L. and Luo, S. (2019) Application of Nanotechnology in the Removal of Heavy Metal from Water. In: Luo, X.B. and Deng, F., Eds., *Nanomaterials for the Removal of Pollutants and Resource Reutilization*, Elsevier, 83-147. https://doi.org/10.1016/b978-0-12-814837-2.00004-4

[24] Al-Rashed, S.M. and Al-Gaid, A.A. (2012) Kinetic and Thermodynamic Studies on the Adsorption Behavior of Rhodamine B Dye on Duolite C-20 Resin. *Journal of Saudi Chemical Society*, **16**, 209-215. https://doi.org/10.1016/j.jscs.2011.01.002

[25] Karatas, M. (2012) Removal of Pb(II) from Water by Natural Zeolitic Tuff: Kinetics and Thermodynamics. *Journal of Hazardous Materials*, **199**, 383-389. https://doi.org/10.1016/j.jhazmat.2011.11.035

[26] De Castro, M.L.F.A., Abad, M.L.B., Sumalinog, D.A.G., Abarca, R.R.M., Paoprasert, P. and de Luna, M.D.G. (2018) Adsorption of Methylene Blue Dye and Cu(II) Ions on Edta-Modified Bentonite: Isotherm, Kinetic and Thermodynamic Studies. *Sustainable Environment Research*, **28**, 197-205. https://doi.org/10.1016/j.serj.2018.04.001

[27] Kubo, A.L., Kremer, L., Herrmann, S., *et al.* (2017) Antimicrobial Activity of Polyoxometalate Ionic Liquids against Clinically Relevant Pathogens. *ChemPlusChem*, **82**, 867-871. https://doi.org/10.1002/cplu.201700251